Estimation of the effective orientation of the SHG source in primary cortical neurons

Sotiris Psilodimitrakopoulos[1], Valerie Petegnief[2], Guadalupe Soria[2], Ivan Amat-Roldan[1], David Artigas[1,3], Anna M. Planas[2], and Pablo Loza-Alvarez[1,*]

[1]*ICFO-Institut de Ciències Fotòniques, Mediterranean Technology Park, 08860 Castelldefels (Barcelona), Spain*

[2] *Department of Brain Ischemia and Neurodegeneration, Institute for Biomedical Research of Barcelona (IIBB), Spanish Research Council (CSIC), Institut d'Investigacions Biomèdiques August Pi Sunyer (IDIBAPS), Barcelona, Spain*

[3] *UPC- Universitat Politècnica de Catalunya, Department of signal theory and communications, 08034, Barcelona, Spain*

**pablo.loza@icfo.es*

Abstract: In this paper we provide, for the first time to our knowledge, the effective orientation of the SHG source in cultured cortical neuronal processes *in vitro*. This is done by the use of the polarization sensitive second harmonic generation (PSHG) imaging microscopy technique. By performing a pixel-level resolution analysis we found that the SHG dipole source has a distribution of angles centered at θ_e =33.96°, with a bandwidth of $\Delta\theta_e$ = 12.85°. This orientation can be related with the molecular geometry of the tubulin heterodimmer contained in microtubules.

OCIS codes: (110.5405) Polarimetric imaging; (170.3880) Medical and biological imaging; (170.6935) Tissue characterization; (180.4315) Nonlinear microscopy; (180.5810) Scanning microscopy; (190.2620) Harmonic generation and mixing; (190.1900) Diagnostic applications of nonlinear optics

References and links

1. P. J. Campagnola, A. C. Millard, M. Terasaki, P. E. Hoppe, C. J. Malone, and W. A. Mohler, "Three – dimensional high-resolution second harmonic generation imaging of endogenous structural proteins in biological tissues," Biophys. J. **82**(1), 493–508 (2002).
2. S. Roth, and I. Freund, "Second harmonic generation in collagen," J. Chem. Phys. **70**(4), 1637–1643 (1979).
3. P. Stoller, K. M. Reiser, P. M. Celliers, and A. M. Rubenchik, "Polarization-modulated second harmonic generation in collagen," Biophys. J. **82**(6), 3330–3342 (2002).
4. S. W. Chu, S. Y. Chen, G. W. Chern, T. H. Tsai, Y. C. Chen, B. L. Lin, and C. K. Sun, "Studies of $\chi(2)/\chi(3)$ tensors in submicron-scaled bio-tissues by polarization harmonics optical microscopy," Biophys. J. **86**(6), 3914–3922 (2004).
5. S. V. Plotnikov, A. C. Millard, P. J. Campagnola, and W. A. Mohler, "Characterization of the myosin-based source for second harmonic generation from muscle sarcomeres," Biophys. J. **90**, 693–703 (2006).
6. F. Tiaho, G. Recher, and D. Rouède, "Estimation of helical angles of myosin and collagen by second harmonic generation imaging microscopy," Opt. Express **15**(19), 12286–12295 (2007).
7. S. Psilodimitrakopoulos, S. Santos, I. Amat-Roldan, A. K. Thayil, D. Artigas, and P. Loza-Alvarez, "In vivo, pixel-resolution mapping of thick filaments' orientation in nonfibrilar muscle using polarization-sensitive second harmonic generation microscopy," J. Biomed. Opt. **14**(1), 014001–014011 (2009).
8. C. Odin, Y. Le Grand, A. Renault, L. Gailhouste, and G. Baffet, "Orientation fields of nonlinear biological fibrils by second harmonic generation microscopy," J. Microsc. **229**(Pt 1), 32–38 (2008).
9. C. Odin, T. Guilbert, A. Alkilani, O. P. Boryskina, V. Fleury, and Y. Le Grand, "Collagen and myosin characterization by orientation field second harmonic microscopy," Opt. Express **16**(20), 16151–16165 (2008).
10. S. Psilodimitrakopoulos, D. Artigas, G. Soria, I. Amat-Roldan, A. M. Planas, and P. Loza-Alvarez, "Quantitative discrimination between endogenous SHG sources in mammalian tissue, based on their polarization response," Opt. Express **17**(12), 10168–10176 (2009).
11. D. A. Dombeck, K. A. Kasischke, H. D. Vishwasrao, M. Ingelsson, B. T. Hyman, and W. W. Webb, "Uniform polarity microtubule assemblies imaged in native brain tissue by second-harmonic generation microscopy," Proc. Natl. Acad. Sci. U.S.A. **100**(12), 7081–7086 (2003).
12. P. J. Campagnola, M. D. Wei, A. Lewis, and L. M. Loew, "High-resolution nonlinear optical imaging of live cells by second harmonic generation," Biophys. J. **77**(6), 3341–3349 (1999).
13. A. C. Kwan, D. A. Dombeck, and W. W. Webb, "Polarized microtubule arrays in apical dendrites and axons," Proc. Natl. Acad. Sci. U.S.A. **105**(32), 11370–11375 (2008).

#113048 - $15.00 USD Received 18 Jun 2009; revised 22 Jul 2009; accepted 27 Jul 2009; published 31 Jul 2009

14. A. C. Kwan, K. Duff, G. K. Gouras, and W. W. Webb, "Optical visualization of Alzheimer's pathology via multiphoton-excited intrinsic fluorescence and second harmonic generation," Opt. Express **17**(5), 3679–3689 (2009).
15. W. H. Stoothoff, B. J. Bacskai, and B. T. Hyman, "Monitoring tau-tubulin interactions utilizing second harmonic generation in living neurons," J. Biomed. Opt. **13**(6), 064039 (2008).
16. G. Filippidis, C. Kouloumentas, G. Voglis, F. Zacharopoulou, T. G. Papazoglou, and N. Tavernarakis, "Imaging of Caenorhabditis elegans neurons by second-harmonic generation and two-photon excitation fluorescence," J. Biomed. Opt. **10**(2), 024015–024018 (2005).
17. S. Y. Chen, C. S. Hsieh, S. W. Chu, C. Y. Lin, C. Y. Ko, Y. C. Chen, H. J. Tsai, C. H. Hu, and C. K. Sun, "Noninvasive harmonics optical microscopy for long-term observation of embryonic nervous system development in vivo," J. Biomed. Opt. **11**(5), 054022–054028 (2006).
18. C. Odin, C. Heichette, D. Chretien, and Y. Le Grand, "Second harmonic microscopy of axonemes," Opt. Express **17**(11), 9235–9240 (2009).
19. A. Akhmanova, and M. O. Steinmetz, "Tracking the ends: a dynamic protein network controls the fate of microtubule tips," Nat. Rev. Mol. Cell Biol. **9**(4), 309–322 (2008).
20. H. P. Erickson, "Microtubule surface lattice and subunit structure and observations on reassembly," J. Cell Biol. **60**(1), 153–167 (1974).
21. S. Saxena, and P. Caroni, "Mechanisms of axon degeneration: from development to disease," Prog. Neurobiol. **83**(3), 174–191 (2007).
22. K. J. De Vos, A. J. Grierson, S. Ackerley, and C. C. J. Miller, "Role of axonal transport in neurodegenerative diseases," Annu. Rev. Neurosci. **31**(1), 151–173 (2008).
23. K. N. Anisha Thayil, E. J. Gualda, S. Psilodimitrakopoulos, I. G. Cormack, I. Amat-Roldán, M. Mathew, D. Artigas, and P. Loza-Alvarez, "Starch-based backwards SHG for in situ MEFISTO pulse characterization in multiphoton microscopy," J. Microsc. **230**(Pt 1), 70–75 (2008).
24. V. Petegnief, M. Font-Nieves, M. E. Martín, M. Salinas, and A. M. Planas, "Nitric oxide mediates NMDA-induced persistent inhibition of protein synthesis through dephosphorylation of eukaryotic initiation factor 4E-binding protein 1 and eukaryotic initiation factor 4G proteolysis," Biochem. J. **411**(3), 667–677 (2008).
25. O. Nadiarnykh, and P. J. Campagnola, "Retention of polarization signatures in SHG microscopy of scattering tissues through optical clearing," Opt. Express **17**(7), 5794–5806 (2009).
26. A. Erikson, J. Örtegren, T. Hompland, C. de Lange Davies, and M. Lindgren, "Quantification of the second-order nonlinear susceptibility of collagen I using a laser scanning microscope," J. Biomed. Opt. **12**(4), 044002–044010 (2007).
27. I. Freund, M. Deutsch, and A. Sprecher, "Connective tissue polarity. Optical second-harmonic microscopy, crossed-beam summation, and small-angle scattering in rat-tail tendon," Biophys. J. **50**(4), 693–712 (1986).
28. A. Leray, L. Leroy, Y. Le Grand, C. Odin, A. Renault, V. Vié, D. Rouède, T. Mallegol, O. Mongin, M. H. V. Werts, and M. Blanchard-Desce, "Organization and orientation of amphiphilic push-pull chromophores deposited in Langmuir-Blodgett monolayers studied by second harmonic generation and atomic force microscopy," Langmuir **20**(19), 8165–8171 (2004).

1. Introduction

Second harmonic generation (SHG) imaging microscopy of biological samples usually relies on nonlinear excitation with ultrashort pulses, typically in the infrared spectral region, of endogenous non-centrosymmetric molecular structures [1]. The produced SHG signal originates from the laser induced 2nd order polarization in the molecule. In this way, the signal is sensitive to the incoming polarization of the excitation beam and to the SHG active molecular structural conformation [2–4]. Taking advantage of this, it has been demonstrated that by rotating the linear polarization of the beam reaching the sample plane and by analysing the modulated SHG signal, it is possible to gain information, at the molecular level, that is unreachable by common SHG imaging [3]. Polarization SHG (PSHG) microscopy has since then being used to characterize different tissue components such as collagen and muscle. In particular, the effective orientation angles of the molecule containing the SHG source (harmonophore) were provided for collagen and myosin [5–9]. Subsequently these two components were mapped in the same image, enabling their quantitative discrimination without the need of any exogenous markers [10]. Importantly, the estimated angles of the effective orientation of the harmonophores found using PSHG for collagen and muscle were correlated to the helical pitch angle of one polypeptide chain of the collagen triple-helix and to the α-helix of the myosin's coiled coil (myosin tail), respectively [5,6].

A less bright endogenous SHG contrast in mammalian tissue is originated from polarized microtubule assemblies [11]. Thus, SHG images were acquired in the past mainly from mitotic spindles [1], axons in neurons (in isolated cultures, brain slices, and model organisms) [12–17] and axonemes [18]. In particular, the microtubules are key constituents of the cytoskeleton and are involved in numerous cellular functions such as anterograde and retrograde transport of vesicles and organelles within the axon. They are

#113048 - $15.00 USD Received 18 Jun 2009; revised 22 Jul 2009; accepted 27 Jul 2009; published 31 Jul 2009

constructed from heterodimmers of α- and β-tubulin, which assemble into polar, linear protofilaments that form a closed tube [19]. The dimensions of one heterodimmer are 80 Å along the long axis of the microtubule and 51Å in the transversal direction [20]. Microtubules are dynamic structures that become destabilized or form bundles under pathological conditions. It has been reported that disassembly of microtubules contributes to disrupted axonal transport that is associated to several neurodegenerative diseases [21,22]. Therefore, the detection of changes in the microtubules or any other molecular information may be crucial to reflect an early impairment of axonal transport and/or degeneration processes.

In the present study we use a biophysical model to extract the effective orientation angle, θ_e, of the harmonophores in cultured cortical neuronal processes. In particular, the PSHG signal is fitted, point by point, to the biophysical model, forming images with the local value for the different parameters associated to this model. After a filtering process, based on rejecting pixels that do not fit the model to a set value (usually larger than 90%) of the coefficient of determination, r^2 (square of the correlation coefficient), a new image is formed. After that, it is possible to obtain the distribution of the non-rejected pixels with the values for the different parameters of the algorithm, including the distribution of the harmonophores' effective orientation angle (θ_e). This is molecular information that represents, to the best of our knowledge, the first estimation of the effective orientation of the SHG source in neuronal processes, *in vitro*.

2. Materials and methods

2.1 PSHG microscope

The setup is based on an adapted inverted microscope (TE2000-U, Nikon, Japan) with the *y-z* scanning performed by a pair of galvanometric mirrors (galvos) (Cambridge Technology, UK). The whole microscope unit was enclosed in a plastic box, which was heated to control the temperature at 37°C. For the excitation source, we used a Kerr lens modelocked Ti:sapphire laser (MIRA 900f, Coherent, France), with pulses of 160 fs (measured at the sample plane [23]) with a repetition rate of 76 MHz and was operated at a central wavelength of 810 nm. A linear polarizer, followed by a zero order λ/2 wave plate (QWPO-810, CVI Melles Griot) was placed directly after the galvanometric mirrors. The λ/2 plate was put on a motorized rotational stage (AG-PR100, Newport Corporation) allowing control on the fundamental input polarization at the sample plane. A pair of relay lenses was used to ensure that the fundamental beam was filling the back aperture of the 60x, oil immersion (numerical aperture of NA = 1.4) microscope objective lens [plain Apo-Achromatic, Nikon, Japan]. In the forward collection geometry of the microscope, a proper mount and detection unit was implemented. This unit contained an additional collecting objective (identical to the one mentioned before), a long-wave-pass dichroic beamsplitter (FF665, Semrock Inc), a BG39 filter, a 15*nm* FWHM band pass filter centered at 406*nm* (FF01-406/15-25, Semrock Inc) and a PMT (H9305-04, Hamamatsu, France). The objective lens was mounted on a micrometric *3D* translational stage with tilt correction. The backwards detection unit, located through one of the output ports of the microscope, was used for simultaneous collection of backwards propagated SHG signal (if any). It was equipped with the short-wave-pass dichroic beam splitter (FF720, Semrock Inc), a BG39 filter, and the 15*nm* FWHM bandpass filter centered at 406*nm* which was directly placed before an identical PMT. Figure 1 shows a schematic of our experimental setup. A labVIEW interface program was written to control the raster scanning of the galvo-mirrors and the data acquisition (DAQ) card. Typical frame acquisition times for a single 500 x 500 pixels image were about ~1.5*s* (pixel dwell time is ~6μs). The effect of depolarization of the fundamental beam introduced by the different optical components was measured at the sample plane. The extinction coefficient ratio of the fundamental incident light was measured for every polarization, finding the values of 25:1 and 63:1, with and without the used objective, respectively. The mean power entering to the microscope was measured to be around 50-80mW (measured just before the galvos) and the transmission of the whole system was about 10-15%.

#113048 - $15.00 USD Received 18 Jun 2009; revised 22 Jul 2009; accepted 27 Jul 2009; published 31 Jul 2009

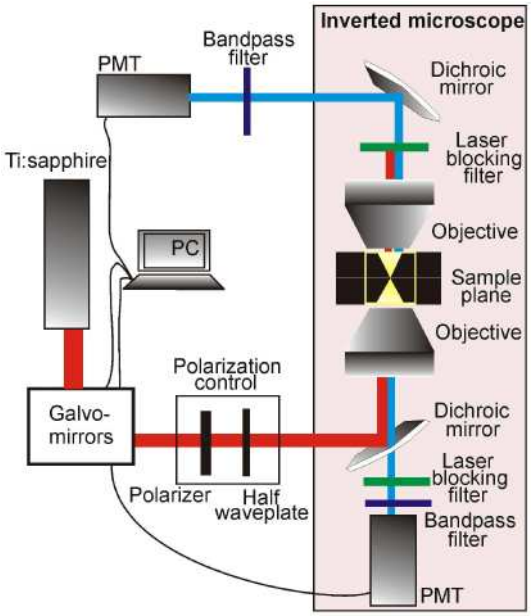

Fig. 1. Block diagram of the experimental optical setup.

2.2 Cultured neurons

Primary cortical neuron cultures were prepared from 18-day-old Sprague–Dawley rat embryos (Charles River Laboratories) as described previously [24]. Briefly, animals were anaesthetized and sacrificed by cervical dislocation. All procedures were approved by the Ethical Committee for Animal Use (CEEA) at the University of Barcelona. Cells were resuspended in MEM supplemented with 10% fetal calf serum and 100 µg/ml gentamycin and plated onto poly-L-lysine (5 µg/ml)-precoated glass bottom dishes at a density of 764 cells/mm^2. Ara-C (cytosine arabinoside) was added on day *in vitro* (DIV) 4 to limit glial proliferation and medium was partly changed on 7 DIV with MEM supplemented with B27 and ARA-C. PSHG imaging in neuronal processes was performed on 7 day-in vitro.

2.3 Theoretical model

Several biophysical models for interpreting the PSHG contrast have been proposed in the past [3,5,25,26]. We are assuming cylindrical symmetry along the microtubule long axis. The cylinder lies in its coordinates system (y-z) plane and it is parallel to laboratory *y'-z'* plane. The laser light propagates along the laboratory *x'*-axis and its linear polarization is rotating in the *y'-z'* plane in an angle α with the z'-axis. With this geometry, the *x'* (lab) and the *x* (cylinder), axes coincide. Then, any rotation between the cylinder and the laboratory frames corresponds to an angle φ. The $\chi^{(2)}$ tensor in the compressed notation for cylindrical geometry where $d_{15}=d_{24}$ and $d_{31}=d_{32}$ (x=y) can be written as:

$$\chi_{ijk}^{(2)} \sim \begin{bmatrix} 0 & 0 & 0 & 0 & d_{15} & 0 \\ 0 & 0 & 0 & d_{24} & 0 & 0 \\ d_{31} & d_{32} & d_{33} & 0 & 0 & 0 \end{bmatrix}.$$

The polarization dependence of SHG intensity, assuming that no axial field components are introduced by the objective and kleinmans's symmetry ($d_{31}= d_{15}$), can be described by [27]:

$$I_{SHG} \sim \{[\sin 2(\alpha-\varphi)]^2 + [\sin^2(\alpha-\varphi) + d_{33}/d_{15}\cos^2(\alpha-\varphi)]^2\}. \qquad (1)$$

#113048 - $15.00 USD Received 18 Jun 2009; revised 22 Jul 2009; accepted 27 Jul 2009; published 31 Jul 2009

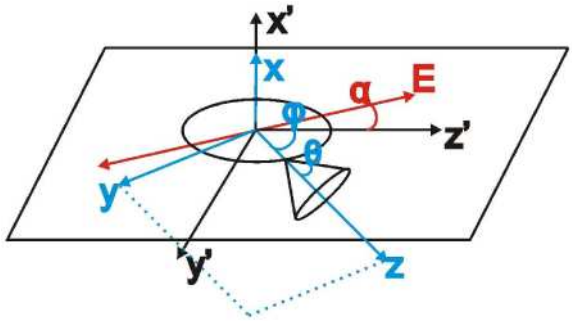

Fig. 2. Coordinates system of the theoretical model.

The next step consists in obtaining the relationship between the nonvanishing elements of the $\chi^{(2)}$ tensor and the effective orientation of the SHG source (see Fig. 2) [5,6]. Here, we consider further assumptions about the relation between the hyperpolarizability and macroscopic tensors. First, a single axis SHG source with dominant hyperpolarizability $\beta^{(2)}_{vvv}$ along the axis-v in a (μ, ξ, v) microscopic molecular coordinates system is considered. The $\chi^{(2)}$ tensor is then related with the hyperpolarizability as: $d_{ijk} \sim N\left\langle (\hat{i}\hat{v})(\hat{j}\hat{v})(\hat{k}\hat{v})\right\rangle \beta^{(2)}_{vvv}$, where N is the density of sources and $\langle\ \rangle$ denotes their average orientation. Second, by assuming a random distribution of source molecules in the azimuth angle, the components of Eq. (1) can be expressed in terms of the angle θ between $\beta^{(2)}_{vvv}$ and the microtubule long axis as: $d_{33} = d_{zzz} = N\left\langle \cos^3\theta \right\rangle \beta^{(2)}_{vvv}$, and $d_{15} = d_{31} = N\left\langle \cos\theta \sin^2\theta \right\rangle \beta^{(2)}_{vvv} / 2$. Finally, we consider that in the focal volume (transversal resolution is ~ 600nm, corresponding to ~3 pixels) the angular distribution of the source molecule, θ, and the microtubule orientation, φ, are narrow (then, the symbol $\langle\ \rangle$ can be removed). Therefore, the angle θ coincides with the effective orientation angle θ_e of the SHG source molecule and can be obtained from the nonvanishing elements of the $\chi^{(2)}$ tensor as [28]:

$$\cos^2\theta_e = \frac{d_{33}/d_{15}}{2 + d_{33}/d_{15}}. \tag{2}$$

2.4 Fitting method

Equation (2) gives the key parameter θ_e that is used for estimating the effective orientation of the SHG source. Therefore, the objective is to retrieve the coefficients ratio given by $b = d_{33}/d_{15}$. For analysis purposes, Eq. (1) is rewritten as:

$$I^{2\omega} = E\left\{\sin^2 2(\varphi-\alpha) + [\sin^2(\varphi-\alpha) + b\cos^2(\varphi-\alpha)]^2\right\} + \delta, \tag{3}$$

where, the free parameters E, φ, b, and δ are retrieved using a fitting algorithm based on a nonlinear least-squares fitting routine (The Mathworks, Champaign-Urbana, IL) using four hundred iterations per pixel. It has to be noted that Eq. (3) has an extra parameter δ in comparison to Eq. (1). This parameter has been added to include both experimental errors and any deviation from the theoretical model as described in [7,10]. The algorithm runs for nine different angles α of the incoming polarization (from 0° to 160° in steps of 20°), where the intensity value for a given polarization is composed by the averaged raw data values among three different images. In addition, since all the terms in Eq. (3) are positive, the algorithm is forced to retrieve positive real values for all the parameters in the equation.

3. Results and discussion

We started by carrying out PSHG imaging in neuronal processes of primary cultured neurons. The mean power reaching the sample plane was 8.5mW. In this regime no

#113048 - $15.00 USD Received 18 Jun 2009; revised 22 Jul 2009; accepted 27 Jul 2009; published 31 Jul 2009

observable damage occurred in the cultured neurons for long imaging periods of time (~30 min.). Figure 3 shows the SHG images acquired for each fundamental linear polarizations. In a previous work, we have shown that the number of polarizations used in the fitting algorithm notably affects the accuracy of the retrieved parameters, 9 polarizations being adequate for our quantification purpose [10]. From Fig. 3, we can observe that maximum signal is detected when the incoming linear polarization is parallel to the neuronal processes and minimum SHG signal when it is perpendicular to them.

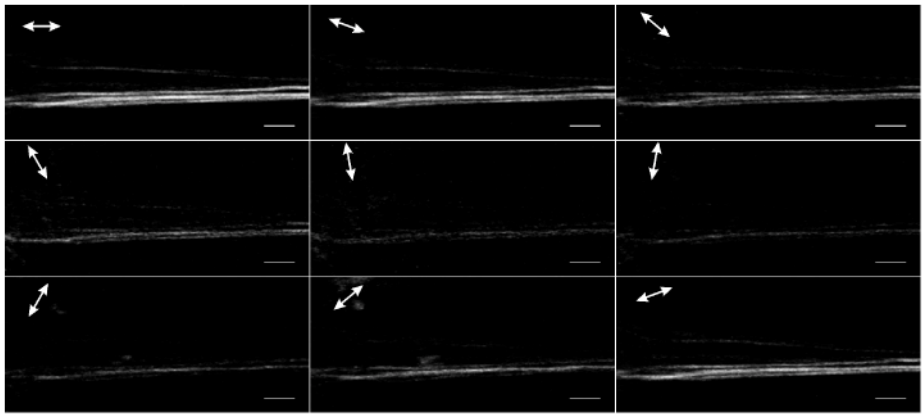

Fig. 3. Polarization dependent SHG imaging microscopy of cultured primary cortical neurons. The incoming linear polarization is rotating clockwise between 0° - 160°, in steps of 20°. Arrows indicate the incoming polarization. Scale bar (on the right bottom corner of each panel) represents 10μm.

With the above images, we then proceed to run the algorithm in which every pixel was fit to the model (Eq. (3)). Erroneous pixels were removed by keeping those with a coefficient of determination (r^2) above 90% (see Fig. 4). The results for the free parameters of Eq. (3) are summarized in Table 1.

Table 1. The values of the parameters θ_e δ, b, E, φ, of Eq. (3) The different values are the *mean*, and the standard deviation (2σ) of a Gaussian distribution fit for the obtained histograms with pixels with r^2>90% in the ROI indicated in Fig. 4(a).

(r^2>90%)	θ_e	$\Delta\theta_e$	δ	$\Delta\delta$	b	Δb	E	ΔE	φ	$\Delta\varphi$
	33.96°	12.85°	0.05	0.10	4.41	2.95	0.01	0.06	2.54°	1.77°

The physical meaning of each parameter is: i) δ is a correction factor for the imperfections in the experimental setup and the model assumptions, ii) b denotes the ratio d_{33}/d_{15}, iii) E is an amplitude, related with the SHG efficiency conversion, and iv) φ is the angle of the long axis of the cylinder (microtubule) with respect to the lab (x') coordinate system (Fig. 2). The PSHG analysis was performed in 4 neuronal processes and in all the cases the results were consistent with the values presented here (data not shown). Figure 4(a) shows the resulting image by plotting the retrieved b parameter. Figs. (b)-(e) show the histograms for the parameters b, E, δ, and φ, respectively. Finally, in Fig. 4(f), we present examples of the fit of three different pixels with different b values (b=2.45, 4.43 and 7.77).

#113048 - $15.00 USD Received 18 Jun 2009; revised 22 Jul 2009; accepted 27 Jul 2009; published 31 Jul 2009

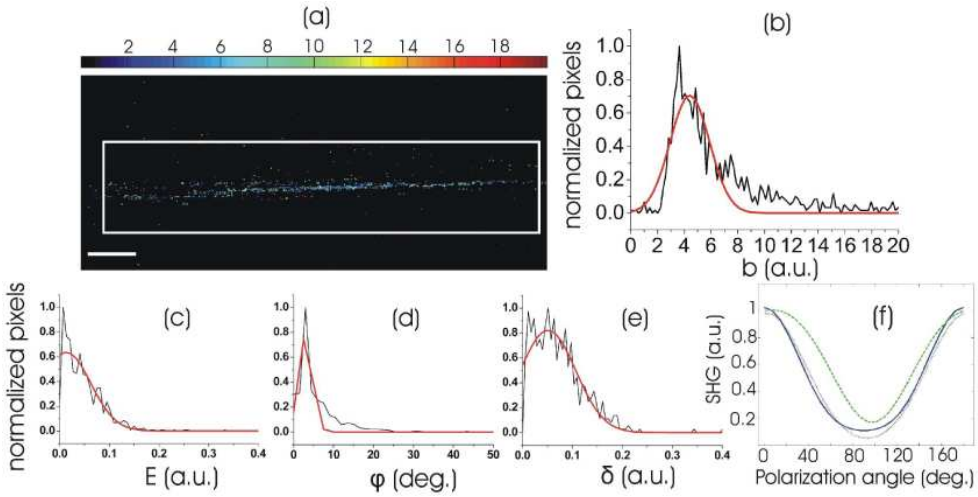

Fig. 4. (a) Resulting image of the b parameter for those pixels with r^2>90% (scale bar is 10μm). (b)-(e) Histograms of the different parameters (within the same ROI of Fig. 4(a)) for b, E, δ and φ, respectively. The red line in each figure is a Gaussian fit to each of the histograms. (f) Examples of the fit of three different pixels. The retrieved parameters are: light grey line b=4.43, E=0.05, φ=2.64, δ=0; green dashed-line b=2.46, E=0.17, φ=7.44, δ=0; blue line b=7.77, E=0.02, φ=0, δ=0.09.

With the values obtained for the b parameter, the effective orientation θ_e of the harmonophores is calculated, for every pixel, using Eq. (2). The resulting distribution was found to be centred at θ_e=33.96° with a width $\Delta\theta_e$ =12.85. Our results present, for the first time, the effective orientation of the harmonophores responsible of the SHG response of the microtubules in cultured cortical neurons. This agrees well with a related previous work [18]. Furthermore, harmonophore orientation has previously been related with structural aspects of the analyzed molecule. In the case of collagen and muscle, the found SHG effective angles were attributed to the helical pitch angle of one collagen polypeptide helix and to the α-helix of the myosin's tail, respectively [5–7,10]. In order to relate our result with some structural aspect in neuronal processes, we look at the tubuline heterodimmer. As mentioned in the introduction, the reported dimensions of one tubuline heterodimmer are 51Å in the transversal direction and 80 Å along the long axis of the microtubule [20]. Then, the diagonal of the rectangle containing the heterodimmer is at an angle of 32.52°. This angle coincides with the found harmonophore angular orientation indicating its orientation within the microtubule.

4. Conclusions

PSHG technique allowed us to correlate the effective orientation of the SHG source in microtubules in culture cortical neurons, with the geometrical characteristics of the tubuline heterodimmer. The information was obtained by analysing the SHG intensity variation on the incoming polarization and by fitting the experimental data into a biophysical model that assumes cylindrical symmetry in the $\chi^{(2)}$ tensor of the SHG source architectures. The retrieved values were used to estimate the effective orientation of the SHG active source by assuming a single-axis source molecule. Our results showed that the distribution of the effective orientation of the SHG active source in cultured primary cortical neurons was centered at θ_e= 33.96°, with a width of $\Delta\theta_e$= 12.85°. This angle value coincides with the diagonal of the rectangle containing the tubulin heterodimmer with respect to the long axis of the microtubule. To the best of our knowledge, this is the first estimation of the harmonophore effective orientation in neurons. Since changes in θ_e can be monitored with optical techniques, modifications on the θ_e or $\Delta\theta_e$, can be a valuable and powerful technique to assess neuron plasticity as well as disease progression.

#113048 - $15.00 USD Received 18 Jun 2009; revised 22 Jul 2009; accepted 27 Jul 2009; published 31 Jul 2009

Acknowledgments

This work is supported by the Generalitat de Catalunya and by the Spanish government grant TEC2006-12654. Authors also acknowledge The Centre for Innovacio i Desenvolupament Empresarial - CIDEM (RDITSCON07-1-0006), Grupo Ferrer and the European Regional Development Fund. This research has been partially supported by Fundació Cellex Barcelona.

#113048 - $15.00 USD Received 18 Jun 2009; revised 22 Jul 2009; accepted 27 Jul 2009; published 31 Jul 2009